Journal of Membrane Science 504 (2016) 230–239

Contents lists available at ScienceDirect

Journal of Membrane Science

journal homepage: www.elsevier.com/locate/memsci

Dry–wet phase inversion block copolymer membranes with a minimum evaporation step from NMP/THF mixtures

Erik J. Vriezekolk, Kitty Nijmeijer, Wiebe M. de Vos *

Membrane Science & Technology, MESA+ Institute for Nanotechnology, University of Twente, P.O. Box 217, 7500 AE Enschede, The Netherlands

ARTICLE INFO

Article history:
Received 21 October 2015
Received in revised form
3 December 2015
Accepted 29 December 2015
Available online 12 January 2016

Keywords:
Block copolymer membranes
Phase inversion
Self-assembly
Isoporous

ABSTRACT

Block copolymer (BCP) membranes are a very promising new type of membranes, but often have a difficult fabrication method that involves a long evaporation step prior to phase inversion. In this work, we study new novel BCP phase inversion recipes for the fabrication of asymmetric membranes with a thin, ordered isoporous selective layer on top of a highly interconnected porous support layer. A key aim is to shorten the evaporation time while simultaneously allowing the formation of even thinner selective top layers. Asymmetric membranes were fabricated via the combination of polystyrene-*block*-poly(4-vinyl pyridine) self-assembly, solvent evaporation and liquid induced phase separation. Using a solvent mixture of THF and NMP, a selective top layer of just 60 nm thick was formed with an ordered honeycomb-like pore structure. The formed structure depended on several parameters, such as THF/NMP ratio, polymer concentration of the polymer solution and the duration of solvent evaporation. When a high THF/NMP ratio was used (more THF than NMP) the solvent evaporation step could be reduced to only 1 s, a clear advantage when considering scale up of this approach. The THF/NMP ratio also influenced the morphology of the support layer, which translated into a variety of permeabilities (270–1320 L m^{-2} h^{-1} bar^{-1}). Filtration experiments showed that the different top layer structures result in different filtration performance, with more ordered pores resulting in more selective filtration.

1. Introduction

Self-assembling block copolymers (BCPs) are considered to be very promising for the production of nanoporous membranes, since their ability to self-assemble can lead to membranes with very ordered and uniform pores in the range of 10–40 nm [1]. These characteristics can overcome the drawbacks of commercial ultrafiltration membranes [2], which are either very permeable but not selective (polydisperse pores) or selective but not that permeable (low porosity) [3]. Self-assembling BCPs are macromolecules that consist of blocks of two or more distinct monomers that can self-assemble into a variety of different nanostructures [4]. This self-assembling process is a thermodynamically driven process. The formed morphology depends on the composition and molecular weight of the BCP [5].

Diblock copolymers that form a morphology of hexagonally packed cylinders are interesting to use for membrane fabrication, since these cylinders can easily lead to isoporous nanochannels [6]. Fabrication of selective membranes based on BCPs can be divided into several categories. In the first category, a thin dense BCP film (thickness of ~100 to several hundred nanometers) is fabricated by spin-coating or dip-coating, where the hexagonally packed cylinders are orientated perpendicular to the surface. Pores are formed by removing the cylinders by etching or cleaving [7,8], by removing an additional component that resides in the core of the cylinders [9–12], or by an annealing step [6,13]. The thin nanoporous film acts as the selective top layer of the composite membrane [14]. Although selective membranes have been successfully fabricated, the permeabilities of these membranes are significantly lower than commercial membranes [15,16]. The main reason for these low permeabilities is that the orientation of the cylinders changes deeper inside the film and that the pores are not highly interconnected [14].

Much higher permeabilities have been obtained by fabricating freestanding asymmetric BCP membranes via a combination of a solvent evaporation step prior to phase inversion in a coagulation bath [17–24]. This method, *dry–wet phase separation*, is a common method that is used to fabricate asymmetric ultrafiltration and gas separation membranes that contain a thin selective layer on top of a highly interconnected support layer [25]. For the fabrication of the membrane, a polymer solution is used that consists of a polymer, a volatile solvent and a non-volatile solvent [26]. Often the non-volatile solvent has a higher affinity with the nonsolvent than the volatile solvent. After casting a film, the volatile solvent is

* Corresponding author.
E-mail address: w.m.devos@utwente.nl (W.M. de Vos).

http://dx.doi.org/10.1016/j.memsci.2015.12.069
0376-7388/

allowed to evaporate for a certain time, which results in an increase of polymer concentration at the top of the film. In the case of BCPs this leads to the formation of cylindrical or threadlike micelles, because of their self-assembling properties. The film is then solidified very rapidly by immersing the still liquid film in the coagulation bath. The increased polymer concentration at the top of the film results in a thin top film with a structure of ordered hollow channels on top of a more open porous support layer with highly interconnected pores [27,28].

Unfortunately, a solvent evaporation duration of tens of seconds is required for the ordering of the BCPs [21,29–32]. The downside of the longer solvent evaporation is that the selective top layer will become thicker, which increases its hydraulic resistance and therefore reduces its permeability. It also makes it harder to upscale the process. In this work we study novel BCP phase inversion recipes that have a much shorter evaporation step for the fabrication of asymmetric membranes with a thin, ordered isoporous selective layer on top of a highly interconnected porous support layer. Asymmetric polystyrene-*block*-poly(4-vinyl pyridine) is used as a polymer, which has the ability to self-assemble into a cylindrical morphology. The membranes are fabricated by dry–wet phase separation that involves a very short solvent evaporation step followed by fast liquid induced phase separation. A solvent mixture of volatile tetrahydrofuran (THF) and non-volatile N-methylpyrrolidone (NMP) is used to prepare polymer solutions. This is a common combination for the preparation of asymmetric gas separation and ultrafiltration membranes [33–35], but has not been used for the preparation of highly-ordered BCP membranes. We study the effect of NMP/THF ratio, the polymer concentration and the solvent evaporation duration on the formed structure. Contrary to previous isoporous BCP membranes fabricated with dry–wet phase inversion, we demonstrate that highly ordered isoporous membranes with thin top layers can be fabricated with a very short (~1 s) solvent evaporation step, which makes it more easy to upscale this method to e.g. hollow fiber spinning. The fabricated membranes are characterized by permeability measurements and several filtrations. Finally, because the P4VP chains are pH responsive [36], the permeability of our membranes is tested at different pH values.

2. Experimental

2.1. Materials

Polystyrene-*b*-poly(4-vinyl pyridine) (PS-*b*-P4VP) block copolymer P3910A-S4VP (M_w = 109-*b*-30 kg/mol, PDI = 1.15) was purchased from Polymer Source, Inc., Canada and was used without further purification. Tetrahydrofuran (THF, Sigma Aldrich, analytical grade) and N-methylpyrrolidone (NMP, AcrosOrganics, 99% purity) were used as solvents.

Milli-Q pure water (deionized water purified by a Synergy water purification system of Millipore) was used as nonsolvent for phase inversion and for preparing aqueous filtration solutions.

Silver nanoparticles (diameter of 10 and 30 nm) in a 2 mM sodium citrate solution were purchased from NanoComposix, Czech Republic and were used for filtration experiments. Sodium citrate (tribasic dehydrate, ≥ 99.0% purity, Sigma Aldrich) was used for preparing silver nanoparticle buffer solutions. Bovine serum albumin (BSA, ≥ 98% purity, Sigma Aldrich) was also used for filtration experiments.

Hydrochloric acid (HCl, fuming 38 wt%, Sigma Aldrich) was used to prepare water solutions with different pH values.

Table 1
Overview of compositions of polymer solutions used to fabricate composite membranes.

Solution	Polymer concentration [wt%]	THF/NMP ratio [wt/wt]
1	15	60/40
2	18	0/100
3	18	50/50
4	18	60/40
5	18	70/30
6	21	60/40

2.2. Preparation of composite membranes

PS-*b*-P4VP block copolymers were dissolved in THF and NMP and stirred for several hours at room temperature. The solutions had a polymer concentration of 15, 18 or 21 wt% and a THF/NMP ratio of 0/100, 50/50, 60/40 or 70/30 (wt/wt). Different types of nanoporous BCP films were fabricated by using different polymer solutions. An overview of the compositions of all used polymer solutions is presented in Table 1.

The interaction parameters of the BCP and THF are $\chi_{THF\text{-}PS}$ = 0.35 and $\chi_{THF\text{-}P4VP}$ = 0.60 [37], which indicates that THF is a better solvent for PS than for P4VP. The interaction parameters of the BCP and NMP are $\chi_{NMP\text{-}PS}$ = 0.41 and $\chi_{NMP\text{-}4VP}$ = 0.01 [38], which indicates that NMP is a better solvent for P4VP than for PS.

The polymer solution was cast on a glass plate using a custom made casting-machine with an adjustable casting knife (accuracy of 1 μm). The casting height was set to 200 μm. The film was immersed in a MilliQ-pure water coagulation bath at room temperature, ~1 s after casting (amount of time elapsed checked using a timekeeper). During this immersion step (~1 h) the film solidified and could be subsequently detached from the glass plate.

2.3. Characterization

Scanning electron microscopy (SEM) (Jeol JSM 6010 LA, at 5 kV for magnifications up to × 10,000, and High-Resolution SEM, Zeiss Merlin, at 0.5 kV for higher magnifications) was used to visualize and characterize the membranes. Low magnification SEM samples were dried under vacuum at 30 °C for 24 h and then coated with a thin layer of gold using a Balzer Union SCD 040 sputter device.

SemAfore (Jeol) software was used to measure the pore diameters. The average pore diameter was determined by taking the average of at least 100 pores from at least 3 samples. The error in pore diameter was calculated using standard rules for error propagation.

UV–visible spectroscopy (Cary 300 Scan Varian spectrophotometer) was used to determine the concentration of the silver nanoparticles (wavelength of ~410 nm for 30 nm particles, ~393 nm for 10 nm particles) and BSA (wavelength of ~278 nm) in the retention measurements.

2.4. Permeation experiments

The permeability of the membranes was determined by measuring the flux of Milli-Q pure water at different pressures (0.4–1.2 bar) using a dead-end filtration set-up. A membrane (circular, 2.5 cm in diameter) was placed in a filter holder cell with a volume of 4 cL. The cell was connected to a vessel filled with Milli-Q pure water, which was pressurized by compressed nitrogen.

The permeability (L m^{-2} h^{-1} bar^{-1}) was calculated as the ratio of the flux over the applied pressure:

$$Permeability = \frac{V}{A \cdot t \cdot \Delta P} = \frac{J}{\Delta P}$$

where V is the permeate volume (L), A is the membrane area (m^2), t is the time (h), J is the permeate flux ($L\,m^{-2}\,h^{-1}$) and P is the pressure (bar).

All measurements were performed using at least six different membranes to ensure reproducibility. The average permeability and the standard deviation are reported.

During pH-dependent flux measurements, the equilibration time between measurements of different pH values was 30 min.

2.5. Filtration

The membranes were challenged to 30 nm and 10 nm (diameter) silver nanoparticles and BSA (diameter of roughly 7 nm [39]) filtrations performed at 1.00 ± 0.04 bar using the dead-end filtration set-up described before to determine the corresponding retention. Each component was filtrated individually. Aqueous feed solutions were prepared containing 2 mg/L nanoparticles in 0.02 M sodium citrate (pH=7.6) or 1 g/L BSA (pH=6.8).

The rejection R was determined via:

$$R = \frac{C_{cell} - C_{permeate}}{C_{cell}}$$

where $C_{permeate}$ is the permeate concentration (g/L) and C_{cell} the concentration inside the test cell (g/L). Since the setup ran in dead-end mode, accumulation of the retained solutes caused the concentration in the membrane cell to rise in time. Since it was not possible to monitor the concentration inside the cell in time, the average of the original feed concentration and the final retentate concentration was used as C_{cell}. During every filtration experiment, 10–20 ml permeate was collected, of which the first 5 ml was discarded in order to prevent influence of remaining water in the dead volume under the membrane.

3. Results and discussion

3.1. Fabrication and characterization of membranes

We started with fabricating a membrane from a 18 wt% polymer in NMP solution. NMP is a solvent that is frequently used to fabricate membranes via phase inversion with water as non-solvent. After casting, the film was immediately immersed in the coagulation bath, which resulted in a minimized evaporation step of approximately 1 s. This resulted in a very porous membrane with pores of 10–30 nm at the surface (Fig. 1a). The structure of the membrane changed when THF was added to the polymer solution, while keeping the polymer concentration constant. The BCP polymers started to form a more cylindrical threadlike structure when a THF/NMP ratio of 50/50 was used as solvent (Fig. 1b). When the THF/NMP ratio was increased even further to 60/40, the cylindrical threads started to form an ordered structure with more monodisperse pores (Fig. 1c). Using a solvent mixture of 70/30 THF/NMP a well-ordered honeycomb-like structure was obtained

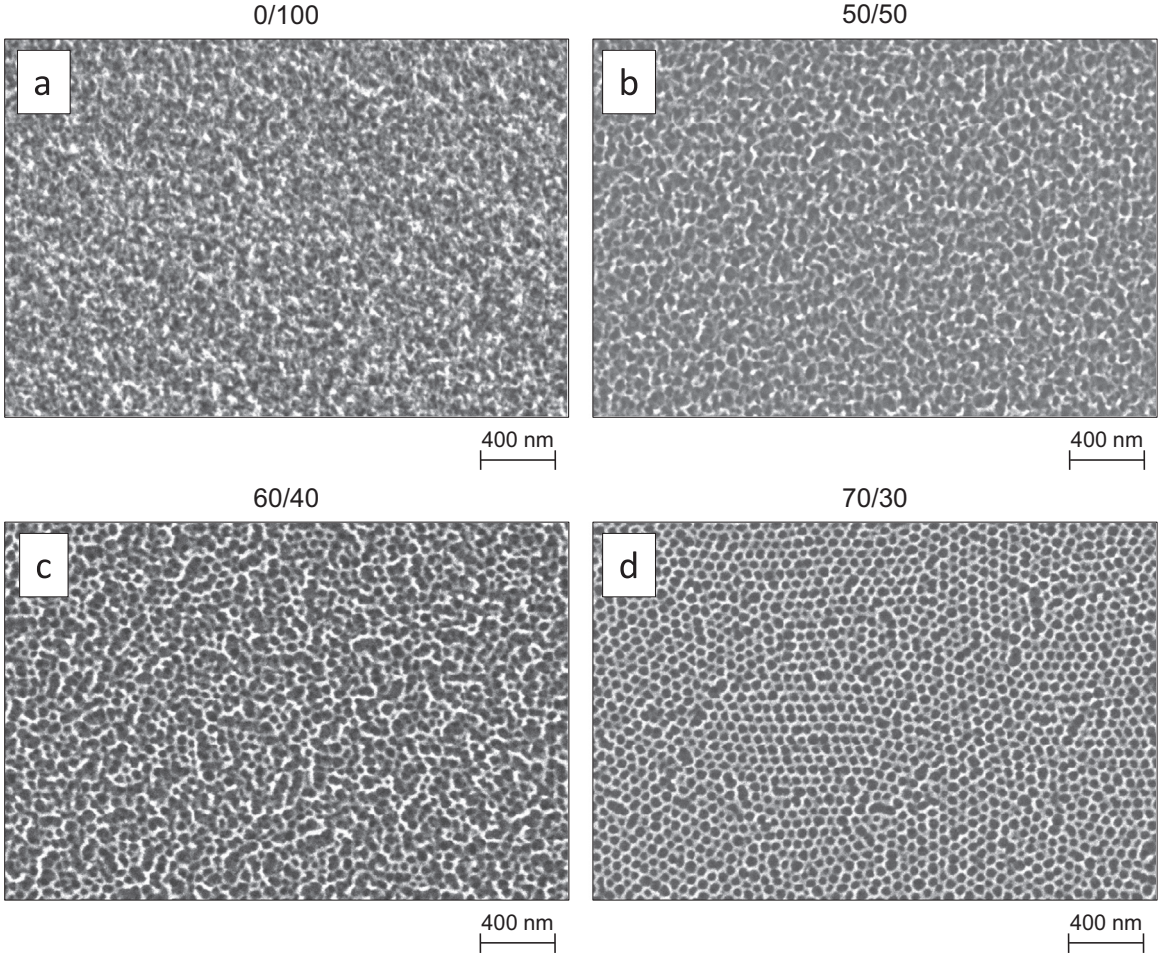

Fig. 1. SEM surface images (magnification= × 100,000) of PS-*b*-P4VP membranes made of 18 wt% polymer solutions with different THF/NMP ratios. (a) 0/100, (b) 50/50, (c) 60/40 and (d) 70/30.

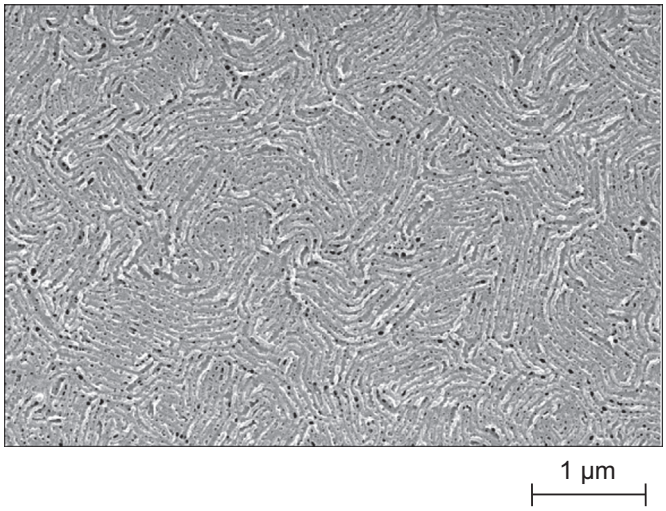

Fig. 2. SEM surface image of a PS-*b*-P4VP membranes made of 18 wt% polymer solutions with a THF/NMP ratio of 60/40 (w/w), and 10 s of solvent evaporation prior to liquid phase inversion.

with pores of sizes of 38 ± 7 nm and a surface porosity of 0.39 (Fig. 1d). The improved structure of the 70/30 membrane seems mainly caused by a smoother surface. While the honeycomb-structure seems flat, the surface of the 60/40 membrane shows elevations where some cylindrical threads are situated higher than others. All membranes, however, showed a defect-free surface. Even higher THF concentrations (80/20) were also investigated, but resulted in gels unsuitable for casting membranes.

Ordered nanoporous structures from BCPs have been fabricated before via dry–wet phase inversion, using different combinations of solvent composition, polymer concentration and the duration of solvent evaporation [29,40]. However, in our case, the presence of THF seems vital for the formation of the ordered honeycomb-like porous structure. THF is known as a good solvent for the formation of thermodynamic driven PS-*b*-P4VP nanostructures [9,41,42]. It has been used as a co-solvent to fabricate PS-b-P4VP membranes with similar well-ordered surfaces via dry–wet phase inversion, but at significantly lower concentrations [17].

The formation of the ordered pores is attributed to the evaporation step prior to liquid induced phase inversion. Evaporation of the more volatile THF leads to a higher polymer concentration at the top of the casted film where the BCPs start to form micelles. This thermodynamically driven formation of micelles leads to the formation of the ordered honeycomb-like pores. The formation of the BCP micelles can take place within 4 s of solvent evaporation [43], however our membranes were fabricated using only 1 s of solvent evaporation, much shorter than previous reported values [21,29,30]. The polymer solutions in this work that lead to honeycomb-like structures contain significantly higher contents of THF, which is known for the formation of PS-*b*-P4VP micelles [44]. We therefore consider the short evaporation time required to obtain honeycomb like pores, an indication that micelles are already present before the start of phase inversion.

The duration of solvent evaporation also influences the morphology of the top of the film. When the evaporation step was prolonged to 10 s, a structure was obtained with worm-like cylinders that are orientated parallel to the surface and having small pores in between (Fig. 2). The asymmetric PS-b-P4VP polymer

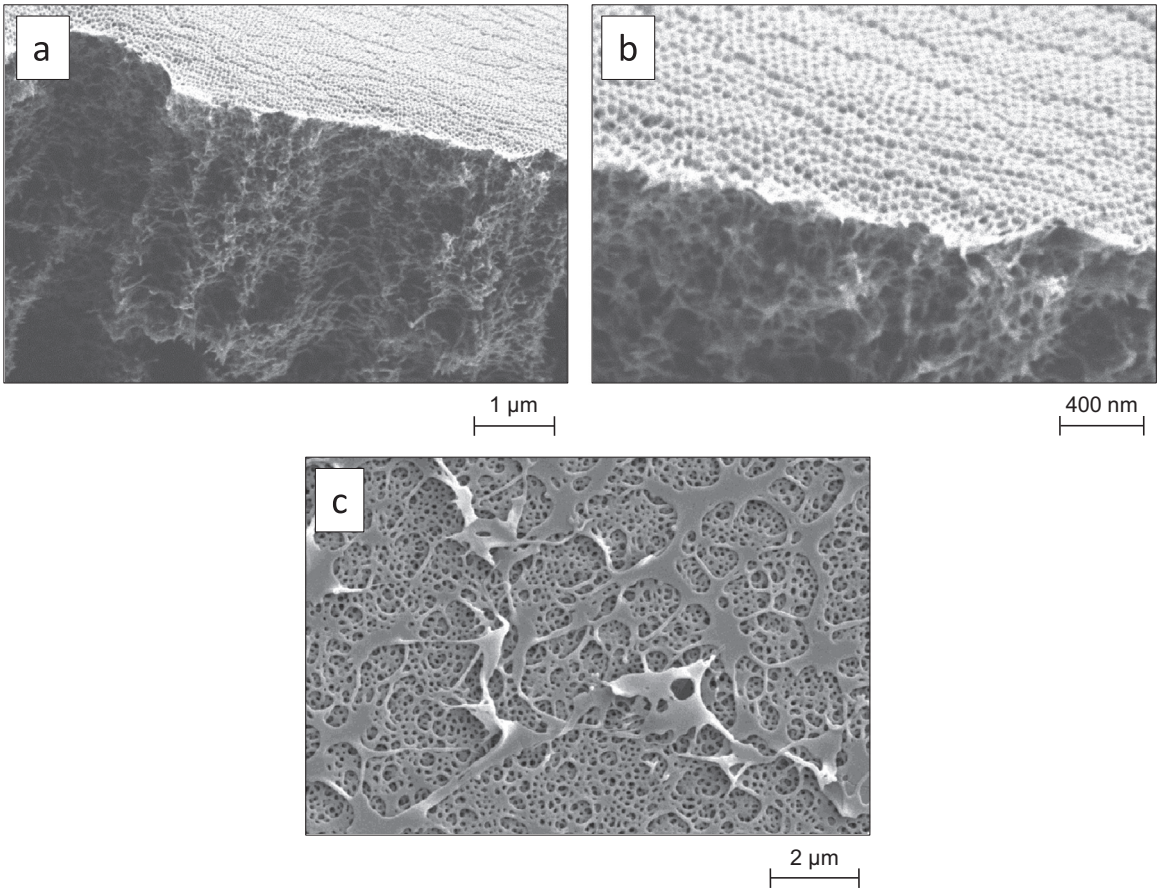

Fig. 3. SEM images of PS-*b*-P4VP membranes made of 18 wt% polymer and a THF/NMP ratio of 60/40. (a) cross-section, magnification $\times$45,000, (b) cross-section, magnification $\times$100,000, (c) bottom, magnification $\times$10,000.

under investigation is known in dense films to form a cylindrical structure, which consists of hexagonally packed cylinders formed by the minority part (P4VP) in a matrix formed by the other part (PS) [45]. When all solvent is allowed to evaporate slowly, a dense structure having this morphology will be obtained. We therefore hypothesize that increasing the evaporation step in our dry–wet phase inversion gives the BCP more time to self-assemble into this structure, leading to the worm-like cylindrical structure that is shown in Fig. 2.

Worm-like cylindrical structures made from polymer solutions that were also used to fabricate ordered porous structures have been observed before [20]. The duration of the evaporation step influences the structure of the top layer [21,29] and in many cases there is an optimum evaporation duration for a given polymer solution [20,40]. In our case, using a 18 wt% polymer solution with a THF/NMP ratio of 70/30, the ideal evaporation duration is very short: only 1 s. This short evaporation step can have significant advantages related to the possibility to scale up BCP membrane production and to produce BCP hollow fiber membranes. In membrane production, the evaporation time needs to be under very controlled conditions (temperature, humidity) to lead to a constant membrane quality, and for a shorter time the conditions are easier to control than for a longer time. For hollow fiber spinning, a long evaporation time can lead to an unacceptably long distance between the spinning head and the coagulation bath or alternatively an unacceptably low spinning speed. Our shorter evaporation time takes away that problem.

Fig. 3 shows the cross-section and the bottom side of a PS-*b*-P4VP membrane made from an 18 wt% polymer solution with a THF/NMP ratio of 70/30. On the cross-section images the porous ordered honeycomb-like structure can be seen on top of a more open sponge-like network of interconnected pores. This asymmetric structure is the result of the combination of the very short solvent evaporation prior to liquid induced phase inversion [25,26]. The thickness of the top-film is just 40–60 nm and of the same order of magnitude as the domain length of the honeycombs. This is thin compared to the thicknesses of BCP top layers found in other asymmetric BCP membranes, which are typically in the range of 100–300 nm [17,19–21, 30,40]. For dry–wet phase separation the thickness of the top layer is determined by the duration of the solvent evaporation step and the ratio of volatile/non-volatile solvent [27,46]. A long solvent evaporation step and a high volatile/non-volatile ratio give rise to a thicker top layer. Therefore the large THF contents used to fabricate our membranes would in principle lead to thick top layers, but this effect is counterbalanced by the very short duration of the evaporation step.

Besides the structure of the selective top layer, also the morphology of the support layer is examined, since the support layer should also be permeable and give the membrane mechanical strength. In Fig. 4, the SEM cross-section images for the four different membranes are shown. The insets show the polymer matrix at a higher magnification. The images show that the THF/NMP ratio not only influences the structure of the top layer, but also

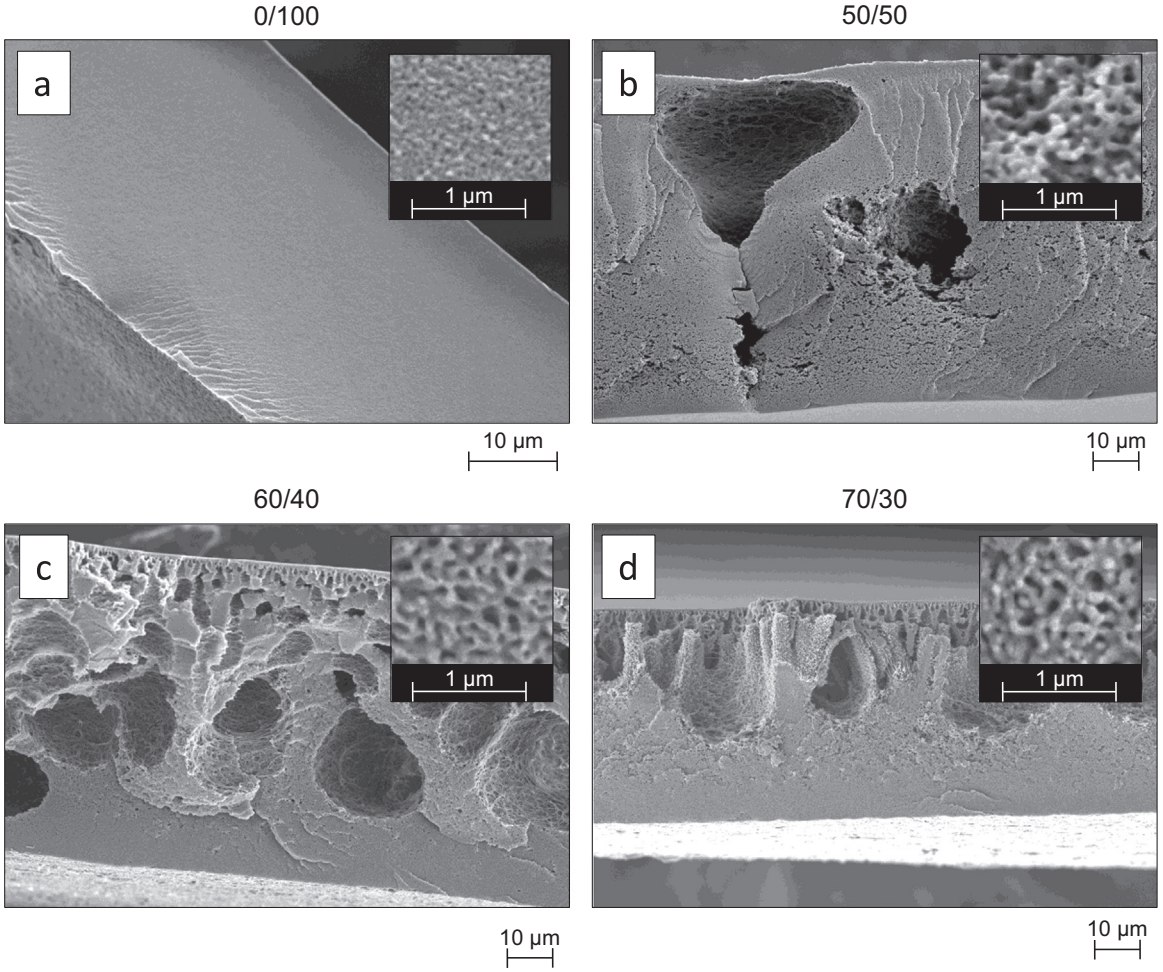

Fig. 4. SEM cross-section images of PS-b-P4VP membranes made of 18 wt% polymer solutions with different THF/NMP ratios. (a) 0/100, (b) 50/50, (c) 60/40 and (d) 70/30. Magnifications are ×2000 (a) and 1000 (b–d). Insets show SEM images zoomed in on the polymer matrix (magnification ×15,000).

influences the morphology of the support layer. Using only NMP as solvent (0/100), a symmetric homogeneous membrane is obtained with an interconnected network of small pores. This morphology looks similar to the structure of the surface (Fig. 1a). This is not surprising, since with the use of only non-volatile NMP no significant solvent evaporation takes place that is required to create an asymmetric layer. The membranes that are fabricated using a mixture of THF and NMP as solvent (Fig. 4b–d) all show a polymer matrix of highly interconnected pores, formed by short worm-like cylinders that are randomly linked with each other. The diameters of these cylinders and the cylinders that form the structures of the top layer seem similar, which suggests that these cylinders are also formed by micelles. Apparently, the BCPs throughout the whole film have the possibility to self-assemble in cylindrical micelles prior to phase inversion. However, the films also have larger voids in the polymer matrix. For the case of the 50/50 membrane, random large and small voids can be seen, as well as cracks that start at these voids. The 60/40 and 70/30 membranes have finger-like pores directly underneath the top layer, which become larger deeper inside the film. These so-called macrovoids are typically seen in ultrafiltration membranes made by phase inversion. They are often found when the solvent and non-solvent have a high affinity and show instantaneous demixing [25]. Surprisingly, in our cases macrovoids start to appear only when high amounts of THF are used, while THF and water are known for delayed demixing [25].

Fig. 5 shows the effect of the polymer concentration on the obtained surface structure of the membrane. The membranes are fabricated using a THF/NMP ratio of 60/40 and an evaporation step of 1 s. When a polymer concentration of 15 wt% is used, a porous structure with a cylindrical micellar structure is obtained (Fig. 5a), but it is less ordered than the honeycomb-like structure obtained using the 18 wt% polymer solution (Fig. 1c). Interestingly, the structure looks very similar as the structure of the membrane fabricated with a 18 wt% polymer solution and a THF/NMP ratio of 50/50 (Fig. 1b). When the polymer concentration is increased to 21 wt% (Fig. 5b) the structure becomes even more ordered than the structure obtained using 18 wt% polymer. Thus, changing the polymer concentration can enhance the ordering of pores. The structure has pores of 35 ± 6 nm and a porosity of 31%. These values are lower than the ordered structure of the 18 wt% 70/30 membrane (Fig. 1d). This can be explained by the higher polymer concentration used to make the structure in Fig. 5b, which normally leads to a more dense morphology in phase inversion [25].

The formation of the structure of the top layer using dry–wet phase inversion is a combination of thermodynamics and kinetics. An interesting theoretical approach has been published that explains the formation of different structures [47]. During the solvent evaporation step, the composition of the BCP, THF and NMP mixture changes continuously. When the film is immersed in the coagulation bath, the solvent concentration decreases because of solvent–nonsolvent exchange, until an unstable composition is reached where the BCP solidifies. The BCP micelles do not freeze instantaneously after immersion of the swollen film in the coagulation, but still have seconds to rearrange to form the final structure [48]. The formed structure depends on this final composition and the path towards it. In this liquid induced phase inversion, the initial composition of the solution is determined by the evaporation step and has a major influence on the path towards solidification. Because two different solvents are used together, the different solvent/nonsolvent pairs should also be considered. The mutual affinity and miscibility of THF and water is lower than that of NMP and water. As a result delayed demixing occurs when THF and water are exchanged, while NMP and water exchange instantly [25]. THF will be more present in PS, since THF does not dissolve P4VP well [49]. Also because water has a more favorable interaction with P4VP than with PS, NMP and water exchange is likely to start in the swollen P4VP domains. In summary, many parameters determine the final structure of the membrane. Unfortunately, a perfect combination of BCP type, suitable solvents, solution composition and duration of solvent evaporation has to be found empirically [47].

Micelle formation is a crucial first step that leads to ordered membrane structures. The state of these micelles, i.e., which blocks form the shell and core, is important since the polymer that forms the shell will determine the surface properties of the membrane. For PS-*b*-P4VP, the state of micellization in a mixed-solvent system has been a point of discussion [50]. It is claimed that P4VP forms the shell of the micelles in a DMF/THF solvent solution when THF starts to evaporate, since the evaporation of THF leads to a higher concentration of DMF, which is more favorable to P4VP [21,22]. However, it was found that thread-like micelles having PS as the shell side are formed in DMF, even though DMF is favorable to P4VP. The incompatibility of the two polymer blocks drives the formation of micelles, having the minority P4VP blocks as micelle core [50]. It is likely that PS also forms the shell side of the micelles in our case. The used BCP also has a majority PS block, and the used polymer solutions contain a high concentration of THF, which is PS favorable. It is possible that with different ratios of NMP/THF one could also form micelles with PS cores and P4VP shells, but this is beyond the scope of the manuscript.

To conclude this paragraph, PS-*b*-P4VP membranes are fabricated using different THF/NMP ratios as solvent. A very short

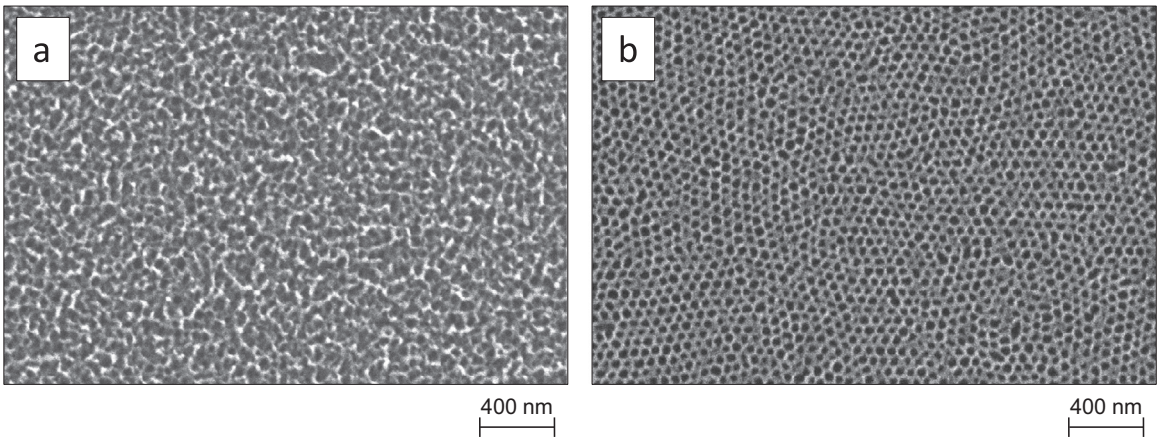

Fig. 5. SEM surface images (magnification = × 100,000) of PS-*b*-P4VP membranes made of (a) 15 wt% polymer solution and (b) 21 wt% polymer solution. Both solutions were made using a THF/NMP ratio of 60/40.

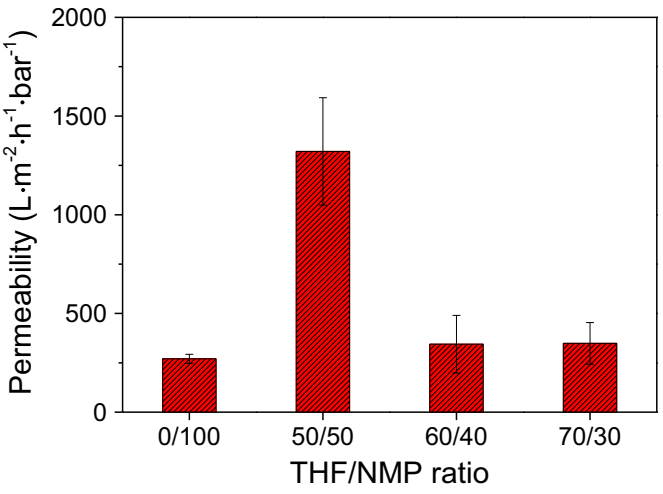

Fig. 6. Permeabilities (pure water) of membranes made with solutions with different THF/NMP weight ratios.

solvent evaporation step prior to precipitation coagulation is required to fabricate an asymmetric membrane with a thin top layer. The THF/NMP ratio and polymer concentration dramatically change the structure of both the top layer and the support layer. In the next paragraphs the effect of the formed structure on the permeability and actual filtration properties will be examined.

3.2. Membrane performance

In all experiments the freestanding membranes were placed on top of a non-woven that acted as an additional mechanical support. Because of the relatively large voids of the non-woven and its high permeability ($\sim$750,000 L m^{-2} h^{-1} bar^{-1}, as determined experimentally) it is assumed that the non-woven has no influence on the results of both the permeability and filtration experiments.

Fig. 6 shows the pure water permeability of membranes made with 18 wt% polymer solutions with different THF/NMP ratios.

A permeability of 270 L m^{-2} h^{-1} bar^{-1} is obtained when pure NMP (0/100) is used. The permeability dramatically increases to $\sim$1320 L m^{-2} h^{-1} bar^{-1} when the THF/NMP ratio is increased to 50/50. When the THF content is further increased to 60/40 and 70/30, the permeability decreases again to 344 and 349 L m^{-2} h^{-1} bar^{-1}, respectively. Although these permeabilities differ a lot, they all are in the range of permeabilities of other freestanding BCP membranes made by phase inversion (40–3000 L m^{-2} h^{-1} bar^{-1} [17,18,40,51]). The thicknesses δ of all fabricated membranes are in the same order of magnitude ($\delta \approx$ 87 μm, 77 μm, 75 μm and 66 μm for THF/NMP=0/100, 50/50, 60/40 and 70/30, respectively), which indicates that the large differences in permeabilities are mainly the result of differences in the membrane structure. Since the hydraulic resistance of the membranes will be mainly caused by the support layer [18], it is best to explain the permeabilities with the SEM cross-section images in Fig. 4. The structure of the 0/100 membrane is denser and has smaller voids than the membranes that were fabricated with THF in the polymer solution. This explains the lowest obtained permeability for this type of membrane. When THF is added to the polymer solution, the polymer matrix shows an interconnected network of pores formed by worm-like tubes. A THF/NMP ratio of 50/50 also shows large voids and cracks in the polymer matrix, which have a very low hydraulic resistance. This is most probably the reason for the very high permeability of 1320 L m^{-2} h^{-1} bar^{-1}. It should nevertheless be noted that this membrane (50/50) was very fragile and therefore difficult to work with. When higher THF contents (60/40 and 70/30) are used, structures with fingerlike macrovoids are formed. Such structures are often seen in other membranes made by phase inversion. These structures normally also have denser regions that decrease the permeability. As these membranes do not show any cracks within the polymer matrix, the permeability is lower than that of the 50/50 membrane.

As shown in this paragraph, the different morphologies of the polymer matrices result in different permeabilities. However, since all morphologies consist of interconnected pores, the permeabilities of all membranes are high. Since the permeability is also determined by the thickness of the membrane, higher permeabilities would be possible by fabricating thinner membranes on top of other support materials. This, however, is beyond the scope of this article.

Fig. 7 shows the rejection of 30 and 10 nm silver nanoparticles

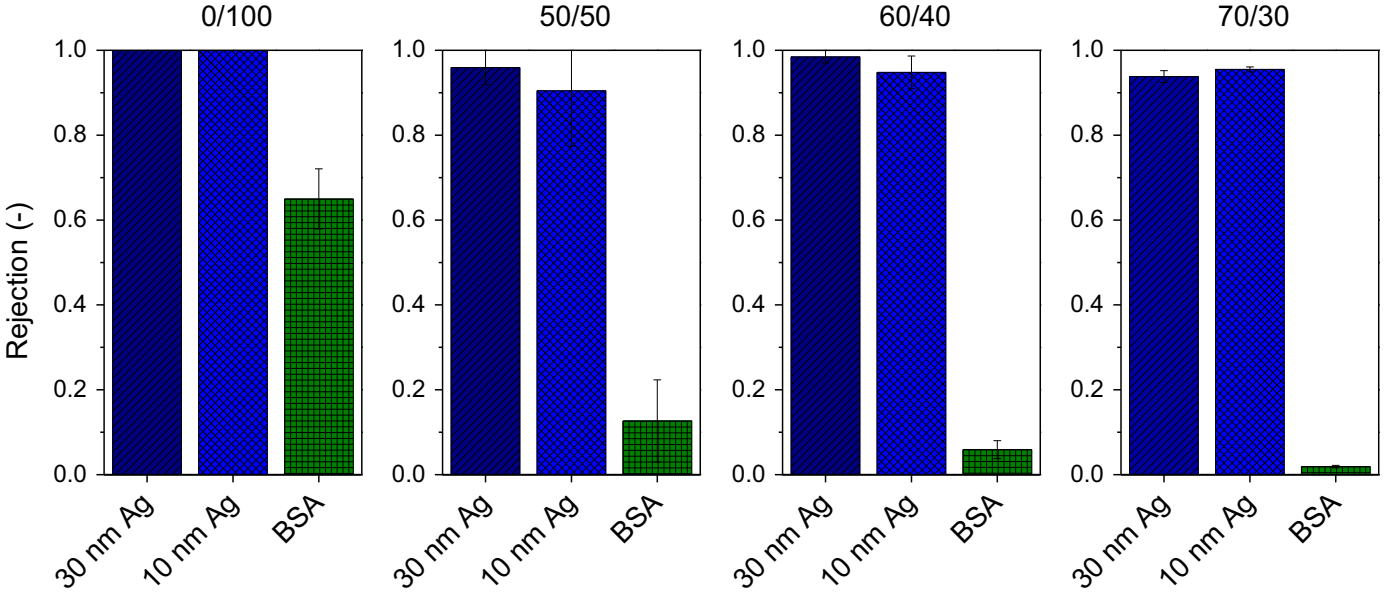

Fig. 7. Rejection of 30 and 10 nm silver nanoparticles and BSA using membranes fabricated with polymer solutions with THF/NMP ratios of 0/100, 50/50, 60/40 and 70/30. Filtrations were performed in a dead-end setup at 1.0 bar.

and BSA for the membranes fabricated with different THF/NMP solvent ratios. Because the filtrations were performed in a dead-end setup, it is expected that accumulation of rejected solutes in the cell module influences the performance of the membrane in time in terms of permeability and rejection. Therefore, only the first 10–20 ml of permeate (of which the first 5 ml was not taken into account) were used for analysis.

The 0/100 membrane completely rejects both 30 and 10 nm silver nanoparticles and has a BSA rejection of 0.65. The membranes made with THF/NMP mixtures never show complete rejection of the nanoparticles, but always have a rejection between 0.90 and 0.98. However, the BSA rejection is much lower compared to the 0/100 membrane, with BSA rejections of 0.13 for the 50/50 membrane, and even lower values of 0.06 and 0.02 when the THF/NMP ratio is increased to 60/40 and 70/30, respectively. The differences in rejections for the different membranes are the result of the different structures of the top layer of the membrane. Although the structure of the 0/100 membrane is less ordered compared to the membranes made with a THF/NMP mixture, the pores are much smaller. Therefore the 0/100 membrane rejects smaller particles, including BSA that has a diameter of ~7 nm [39]. For the membranes made with THF/NMP mixtures one would expect a sharper size cut-off for the membrane with a more ordered pore structure. Indeed, the 70/30 membrane shows a higher difference between the rejections of the 10 nm nanoparticle and BSA than the 50/50 and 60/40 membranes, which means that the pore size distribution is smaller when the pore structure is more ordered. This again demonstrates the key advantages of the BCP membranes, i.e. the ordered pores proved to have a high selectivity and a high porosity.

Fig. 8a shows the flux response of the BCP membranes at different pH values. When the pH is lowered from 6 to 4 the flux remains similar, but decreases dramatically when the pH is further decreased to 3, 2 and 1. The original flux is restored when the pH is increased back to 6. This phenomenon is analogous to other membranes prepared with PS-*b*-P4VP [21,22,30,51,52].

P4VP responds to changes in pH via protonation and deprotonation of the pyridyl group [53]. In the protonated state (below the pK_a of 5.2), the polymer chains are in an extended conformation because of electrostatic repulsion of the charged pyridyl groups, while the chains are coiled in the deprotonated state [54,55]. These conformations respond to a swollen state and a collapsed state of the polymer chains [56]. As a result, the diameter of the pores decreases at low pH and consequently leads to a lower permeability of the membrane. It should be noted that protonation of P4VP also leads to a water-soluble hydrophilic state [56,57], however, the decreasing effective pore diameter is the main phenomenon that contributes to the change in permeability.

Fig. 8b shows an HR-SEM image of the surface of the membrane after immersion in the aqueous HCl solution at a pH of 1.5. Although some of the initial honeycomb-like pores still exist, a significant amount of pores seem to have collapsed. This means that these membranes are pH responsive in terms of permeability, but are also irreversibly damaged once they operate at low pH values. The reason of the pore collapse lies probably in the micellar state of PS-*b*-P4VP. As mentioned before, it is most likely that (for our membranes) P4VP forms the core of the cylindrical threads. Once this core swells, a collapse of the interconnected network of these cylindrical threads seems inevitable.

4. Conclusions

Different membranes made of self-assembling PS-*b*-P4VP can be fabricated using a combination of solvent evaporation followed by phase inversion. Using a solvent mixture of volatile THF and non-volatile NMP, an asymmetric membrane having a very thin top layer and a highly porous and permeable support layer can be fabricated by using only 1 s of solvent evaporation which is a benefit from a processing and scale-up point of view and which would possibly allow commercially relevant production of BCP hollow fibre membranes.

Changing the ratio of THF/NMP leads to membranes with different structures, hence, different performances. When only NMP is used as solvent, a symmetric porous membrane is fabricated. No selective layer is formed because no solvent evaporation takes place, as NMP is a non-volatile solvent. When a THF/NMP mixture is used as solvent, PS-*b*-P4VP starts to form cylindrical micelles that end up as a network of interconnected cylinders, thereby creating a highly permeable structure of interconnected pores. The short solvent (THF) evaporation step prior to phase inversion is enough to create a very thin selective layer of honeycomb-like ordered pores. The ordering of pores can be optimized by varying parameters such as polymer concentration and THF/NMP ratio. The best structures were obtained using a 18 wt% polymer solution with a THF/NMP ratio of 70/30 and a 21 wt% polymer solution with a THF/NMP ratio of 60/40, though it is likely that more combinations exist that lead to these structures.

The THF/NMP ratio also influences the morphology of the support layer, and determines the permeability of the membrane. Large voids and cracks underneath the defect-free top layer give rise to a high permeability (1320 L m^{-2} h^{-1} bar^{-1} for a 50/50 THF/NMP ratio),

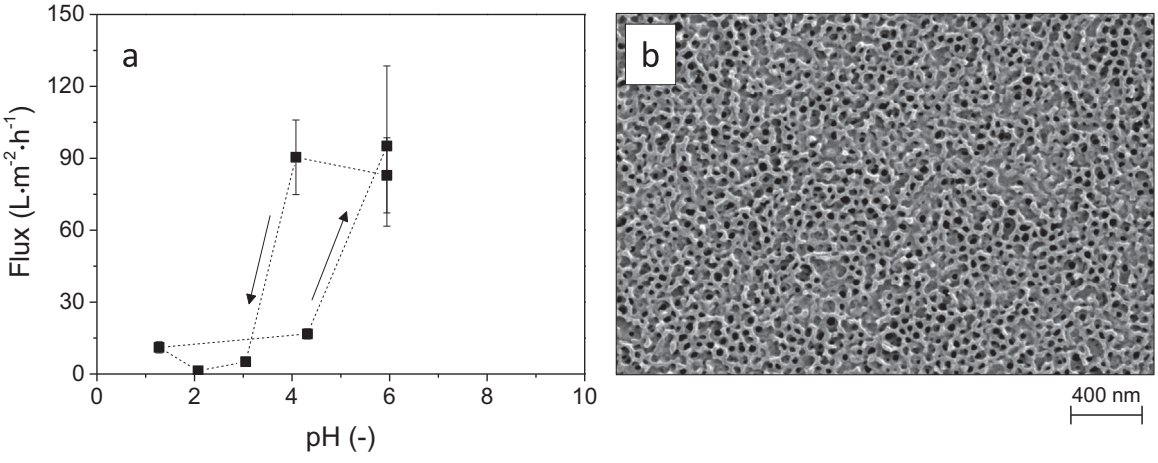

Fig. 8. (a) Flux of a PS-*b*-P4VP membranes made of 18 wt% polymer and a THF/NMP ratio of 60/40 at different pH values. (b) HR-SEM surface image of the membrane after immersion in aqueous HCl solution (pH 1.5).

but make the membrane less mechanically strong. The membrane having the honeycomb-like top layer (70/30) shows a morphology with finger-like macrovoids underneath the top layer, which results in a permeability of 349 L m^{-2} h^{-1} bar^{-1}.

Filtration experiments with 30 and 10 nm silver nanoparticles and BSA show that a sharper size cut-off is obtained when the pores are more ordered. This indicates that the ordered honeycomb-like pores indeed have a lower pore size distribution and result in better filtration performance.

Acknowledgments

This work is supported by NanoNextNL, a micro and nanotechnology consortium of the Government of The Netherlands and 130 partners.

The authors would like to thank Mark A. Smithers (MESA+ Institute, University of Twente) for the High-Resolution SEM imaging.

References

[1] M.M. Pendergast, E.M.V. Hoek, A review of water treatment membrane nanotechnologies, Energy Environ. Sci. 4 (2011) 1946–1971.
[2] E.A. Jackson, M.A. Hillmyer, Nanoporous membranes derived from block copolymers: from drug delivery to water filtration, ACS Nano 4 (2010) 3548–3553.
[3] A. Mehta, A.L. Zydney, Permeability and selectivity analysis for ultrafiltration membranes, J. Membr. Sci. 249 (2005) 245–249.
[4] J.K. Kim, S.Y. Yang, Y. Lee, Y. Kim, Functional nanomaterials based on block copolymer self-assembly, Prog. Polym. Sci. 35 (2010) 1325–1349.
[5] F.S. Bates, G.H. Fredrickson, Block copolymers-designer soft materials, Phys. Today 52 (1999) 32–38.
[6] J. Yin, X. Yao, J.-Y. Liou, W. Sun, Y.-S. Sun, Y. Wang, Membranes with highly ordered straight nanopores by selective swelling of fast perpendicularly aligned block copolymers, ACS Nano 7 (2013) 9961–9974.
[7] J. Bolton, T.S. Bailey, J. Rzayev, Large pore size nanoporous materials from the self-assembly of asymmetric bottlebrush block copolymers, Nano Lett. 11 (2011) 998–1001.
[8] T. Thurn-Albrecht, R. Steiner, J. DeRouchey, C.M. Stafford, E. Huang, M. Bal, M. Tuominen, C.J. Hawker, T.P. Russell, Nanoscopic templates from oriented block copolymer films, Adv. Mater. 12 (2000) 787–791.
[9] W. Lee, X. Zhang, R.M. Briber, A simple method for creating nanoporous block-copolymer thin films, Polymer 51 (2010) 2376–2382.
[10] U. Jeong, D.Y. Ryu, J.K. Kim, D.H. Kim, X. Wu, T.P. Russell, Precise control of nanopore size in thin film using mixtures of asymmetric block copolymer and homopolymer, Macromolecules 36 (2003) 10126–10129.
[11] S.H. Kim, M.J. Misner, T.P. Russell, Solvent-induced ordering in thin film diblock copolymer/homopolymer mixtures, Adv. Mater. 16 (2004) 2119–2123.
[12] E.J. Vriezekolk, E. de Weerd, W.M. de Vos, K. Nijmeijer, Control of pore size and pore uniformity in films based on self-assembling block copolymers, J. Polym. Sci. Part B Polym. Phys. 52 (2014) 1568–1579.
[13] W. Sun, Z. Wang, X. Yao, L. Guo, X. Chen, Y. Wang, Surface-active isoporous membranes nondestructively derived from perpendicularly aligned block copolymers for size-selective separation, J. Membr. Sci. 466 (2014) 229–237.
[14] W.A. Phillip, B. O'Neill, M. Rodwogin, M.A. Hillmyer, E.L. Cussler, Self-assembled block copolymer thin films as water filtration membranes, ACS Appl. Mater. Interfaces 2 (2010) 847–853.
[15] X. Li, C.A. Fustin, N. Lefèvre, J.F. Gohy, S.D. Feyter, J.D. Baerdemaeker, W. Egger, I.F.J. Vankelecom, Ordered nanoporous membranes based on diblock copolymers with high chemical stability and tunable separation properties, J. Mater. Chem. 20 (2010) 4333–4339.
[16] E.J. Vriezekolk, T. Kudernac, W.M. De Vos, K. Nijmeijer, Composite ultrafiltration membranes with tunable properties based on a self-assembling block copolymer/homopolymer system, J. Polym. Sci. 53 (2015) 1546–1558.
[17] K.V. Peinemann, V. Abetz, P.F.W. Simon, Asymmetric superstructure formed in a block copolymer via phase separation, Nat. Mater. 6 (2007) 992–996.
[18] J. Hahn, V. Filiz, S. Rangou, B. Lademann, K. Buhr, J.I. Clodt, A. Jung, C. Abetz, V. Abetz, PtBS-b-P4VP and PTMSS-b-P4VP isoporous integral-asymmetric membranes with high thermal and chemical stability, Macromol. Mater. Eng. 298 (2013) 1315–1321.
[19] J. Hahn, J.I. Clodt, V. Filiz, V. Abetz, Protein separation performance of self-assembled block copolymer membranes, RSC Adv. 4 (2014) 10252–10260.
[20] A. Jung, S. Rangou, C. Abetz, V. Filiz, V. Abetz, Structure formation of integral asymmetric composite membranes of polystyrene-block-poly(2-vinylpyridine) on a nonwoven, Macromol. Mater. Eng. 297 (2012) 790–798.
[21] S.P. Nunes, R. Sougrat, B. Hooghan, D.H. Anjum, A.R. Behzad, L. Zhao, N. Pradeep, I. Pinnau, U. Vainio, K.V. Peinemann, Ultraporous films with uniform nanochannels by block copolymer micelles assembly, Macromolecules 43 (2010) 8079–8085.
[22] S.P. Nunes, A.R. Behzad, B. Hooghan, R. Sougrat, M. Karunakaran, N. Pradeep, U. Vainio, K.V. Peinemann, Switchable pH-responsive polymeric membranes prepared via block copolymer micelle assembly, ACS Nano 5 (2011) 3516–3522.
[23] R.M. Dorin, W.A. Phillip, H. Sai, J. Werner, M. Elimelech, U. Wiesner, Designing block copolymer architectures for targeted membrane performance, Polymer 55 (2014) 347–353.
[24] F. Schacher, M. Ulbricht, A.H.E. Müller, Self-supporting, double stimuli-responsive porous membranes from Polystyrene-block-poly(N,N-dimethylaminoethyl methacrylate) diblock copolymers, Adv. Funct. Mater. 19 (2009) 1040–1045.
[25] M. Mulder, Basic Principles of Membrane Technology, 2nd ed., Kluwer Academic Publishers, Dordrecht, 1996.
[26] S.C. Pesek, W.J. Koros, Aqueous quenched asymmetric polysulfone membranes prepared by dry/wet phase separation, J. Membr. Sci. 81 (1993) 71–88.
[27] A.F. Ismail, P.Y. Lai, Effects of phase inversion and rheological factors on formation of defect-free and ultrathin-skinned asymmetric polysulfone membranes for gas separation, Sep. Purif. Technol. 33 (2003) 127–143.
[28] R.M. Dorin, H. Sai, U. Wiesner, Hierarchically porous materials from block copolymers, Chem. Mater. 26 (2014) 339–347.
[29] J. Hahn, V. Filiz, S. Rangou, J. Clodt, A. Jung, K. Buhr, C. Abetz, V. Abetz, Structure formation of integral-asymmetric membranes of polystyrene-block-Poly(ethylene oxide), J. Polym. Sci. Part B 51 (2013) 281–290.
[30] J.I. Clodt, V. Filiz, S. Rangou, K. Buhr, C. Abetz, D. Höche, J. Hahn, A. Jung, V. Abetz, Double stimuli-responsive isoporous membranes via post-modification of pH-sensitive self-assembled diblock copolymer membranes, Adv. Funct. Mater. 23 (2013) 731–738.
[31] M.M. Pendergast, R. Mika Dorin, W.A. Phillip, U. Wiesner, E.M.V. Hoek, Understanding the structure and performance of self-assembled triblock terpolymer membranes, J. Membr. Sci. 444 (2013) 461–468.
[32] C. Hörenz, C. Pietsch, A.S. Goldmann, C. Barner-Kowollik, F.H. Schacher, Phase inversion membranes from amphiphilic diblock terpolymers, Adv. Mater. Interfaces 2 (2015) 1500042.
[33] M.A. Aroon, A.F. Ismail, M.M. Montazer-Rahmati, T. Matsuura, Morphology and permeation properties of polysulfone membranes for gas separation: effects of non-solvent additives and co-solvent, Sep. Purif. Technol. 72 (2010) 194–202.
[34] J.-J. Shieh, T.S. Chung, Effect of liquid–liquid demixing on the membrane morphology, gas permeation, thermal and mechanical properties of cellulose acetate hollow fibers, J. Membr. Sci. 140 (1998) 67–79.
[35] J. Han, D. Yang, S. Zhang, X. Jian, Effects of dope compositions on the structure and performance of PPES hollow fiber ultrafiltration membranes, J. Membr. Sci. 345 (2009) 257–266.
[36] S. Liu, L. Wang, B. Liu, Y. Song, pH responsiveness of two-layer nano-composite membrane with ultrathin cylindrical nanopores PS-b-P4VP film, Polymer 54 (2013) 3065–3070.
[37] S. Park, J.-Y. Wang, B. Kim, W. Chen, T.P. Russell, Solvent-induced transition from micelles in solution to cylindrical microdomains in diblock copolymer thin films, Macromolecules 40 (2007) 9059–9063.
[38] C.M. Hansen, Hansen Solubility Parameters: A User's Handbook, CRC Press, Boca Raton, 2000.
[39] I. Axelsson, Characterization of proteins and other macromolecules by agarose gel chromatography, J. Chromatogr. A 152 (1978) 21–32.
[40] S. Rangou, K. Buhr, V. Filiz, J.I. Clodt, B. Lademann, J. Hahn, A. Jung, V. Abetz, Self-organized isoporous membranes with tailored pore sizes, J. Membr. Sci. 451 (2014) 266–275.
[41] S. Park, B. Kim, J. Xu, T. Hofmann, B.M. Ocko, T.P. Russell, Lateral ordering of cylindrical microdomains under solvent vapor, Macromolecules 42 (2009) 1278–1284.
[42] S. Roland, D. Gaspard, R.E. Prud'homme, C.G. Bazuin, Morphology evolution in slowly dip-coated supramolecular PS-b-P4VP thin films, Macromolecules 45 (2012) 5463–5476.
[43] D.S. Marques, R.M. Dorin, U. Wiesner, D.-M. Smilgies, A.R. Behzad, U. Vainio, K.-V. Peinemann, S.P. Nunes, Time-resolved GISAXS and cryo-microscopy characterization of block copolymer membrane formation, Polymer 55 (2014) 1327–1332.
[44] S. Roland, C.G. Gamys, J. Grosrenaud, S. Boissé, C. Pellerin, R.E. Prud'homme, C. G. Bazuin, Solvent influence on thickness, composition, and morphology variation with dip-coating rate in supramolecular PS-b-P4VP thin films, Macromolecules 48 (2015) 4823–4834.
[45] E.J. Vriezekolk, E. De Weerd, W.M. De Vos, K. Nijmeijer, Control of pore size and pore uniformity in films based on self-assembling block copolymers, J. Polym. Sci. Part B: Polym. Phys. 52 (2014) 1568–1579.
[46] M. Iqbal, Z. Man, H. Mukhtar, B.K. Dutta, Solvent effect on morphology and CO_2/CH_4 separation performance of asymmetric polycarbonate membranes, J. Membr. Sci. 318 (2008) 167–175.
[47] C. Stegelmeier, V. Filiz, V. Abetz, J. Perlich, A. Fery, P. Ruckdeschel, S. Rosenfeldt, S. Förster, Topological paths and transient morphologies during formation of mesoporous block copolymer membranes, Macromolecules 47 (2014) 5566–5577.
[48] C. Stegelmeier, A. Exner, S. Hauschild, V. Filiz, J. Perlich, S.V. Roth, V. Abetz, S. Förster, Evaporation-induced block copolymer self-assembly into membranes studied by in situ synchrotron SAXS, Macromolecules 48 (2015) 1524–1530.
[49] M. Antonietti, S. Heinz, M. Schmidt, C. Rosenauer, Determination of the micelle architecture of polystyrene/poly(4-vinylpyridine) block copolymers in

dilute solution, Macromolecules 27 (1994) 3276–3281.
[50] L. Oss-Ronen, J. Schmidt, V. Abetz, A. Radulescu, Y. Cohen, Y. Talmon, Characterization of block copolymer self-assembly: from solution to nanoporous membranes, Macromolecules 45 (2012) 9631–9642.
[51] S.P. Nunes, M. Karunakaran, N. Pradeep, A.R. Behzad, B. Hooghan, R. Sougrat, H. He, K.V. Peinemann, From micelle supramolecular assemblies in selective solvents to isoporous membranes, Langmuir 27 (2011) 10184–10190.
[52] R. Hilke, N. Pradeep, P. Madhavan, U. Vainio, A.R. Behzad, R. Sougrat, S. P. Nunes, K.V. Peinemann, Block copolymer hollow fiber membranes with catalytic activity and pH-response, ACS Appl. Mater. Interfaces 5 (2013) 7001–7006.
[53] J. Lindqvist, D. Nyström, E. Östmark, P. Antoni, A. Carlmark, M. Johansson, A. Hult, E. Malmström, Intelligent Dual-responsive cellulose surfaces via surface-initiated ATRP, Biomacromolecules 9 (2008) 2139–2145.
[54] B. Yameen, M. Ali, R. Neumann, W. Ensinger, W. Knoll, O. Azzaroni, Synthetic proton-gated ion channels via single solid-state nanochannels modified with responsive polymer brushes, Nano Lett. 9 (2009) 2788–2793.
[55] N. Ayres, C.D. Cyrus, W.J. Brittain, Stimuli-responsive surfaces using polyampholyte polymer brushes prepared via atom transfer radical polymerization, Langmuir 23 (2007) 3744–3749.
[56] T.K. Tam, M. Ornatska, M. Pita, S. Minko, E. Katz, Polymer brush-modified electrode with switchable and tunable redox activity for bioelectronic applications, J. Phys. Chem. C 112 (2008) 8438–8445.
[57] W. Zhang, L. Shi, R. Ma, Y. An, Y. Xu, K. Wu, Micellization of thermo- and pH-responsive triblock copolymer of poly(ethyleneglycol)-b-poly(4-vinylpyridine)-b-poly(N-isopropylacrylamide), Macromolecules 38 (2005) 8850–8852.